Applied Surface Science 571 (2022) 151256

Contents lists available at ScienceDirect

Applied Surface Science

journal homepage: www.elsevier.com/locate/apsusc

Full Length Article

Atomic layer deposited Pt nanoparticles on functionalized MoS_2 as highly sensitive H_2 sensor

Sungje Lee [a,1], Yunsung Kang [b,1], Jaehyeong Lee [a], Jingyung Kim [b], Jeong Woo Shin [c], Sangjun Sim [b], Dohyun Go [d], Eunhwan Jo [b], Seunghyeon Kye [a], Jongbaeg Kim [b,*], Jihwan An [a,d,*]

[a] Department of Manufacturing Systems and Design Engineering, Seoul National University of Science and Technology, 232 Gongneung-ro, Nowon-gu, Seoul, 01811, Republic of Korea
[b] School of Mechanical Engineering, Yonsei University, 50 Yonsei-ro, Seodaemun-gu, Seoul 03722, Republic of Korea
[c] Department of New Energy Engineering, Seoul National University of Science and Technology, 232 Gongneung-ro, Nowon-gu, Seoul 01811, Republic of Korea
[d] Department of Nano-Bio Engineering, Seoul National University of Science and Technology (SeoulTech), 232 Gongneung-ro, Nowon-gu, Seoul 01811, Republic of Korea

ARTICLE INFO

Keywords:
Molybdenum disulfide
Atomic layer deposition
Plasma treatment
Platinum catalyst
Hydrogen sensor

ABSTRACT

Hydrogen gas (H_2) has garnered significant attention as an alternative clean energy source, and its sensitive detection is essential to prevent explosions due to leakage in storage systems. Molybdenum disulfide (MoS_2), which exhibits a large surface area-to-volume ratio from atomically thin two-dimensional (2D) structure, has attracted attention as a suitable H_2 sensing material. However, pristine MoS_2 exhibits low sensitivity to nonpolar H_2. This paper demonstrates a decoration method for platinum (Pt) catalysts on 2D MoS_2 using atomic layer deposition (ALD) and its application to fabricate highly sensitive H_2 sensors. Additionally, to induce homogeneous distribution of Pt nanoparticles on chemically inert MoS_2 surfaces, oxygen plasma pretreatment is employed as the MoS_2 surface functionalization method. Consequently, highly sensitive detection of H_2 with the sensitivity over 400 and the lower detection limit set to 2.5 ppm, is achieved using ALD Pt-decorated MoS_2, and a sensing mechanism is proposed.

1. Introduction

Two-dimensional (2D) materials have garnered significant attention from researchers owing to interesting electrical, optical, chemical, and/or mechanical properties. Although graphene has been the most widely studied 2D material, other 2D material families such as hexagonal-boron nitride (h-BN), transition metal dichalcogenides (TMDs), along with transition metal carbides and nitrides (MXenes) have been recently studied even more extensively.[1–4] Among such 2D materials, a few layered molybdenum disulfide (MoS_2) nanosheets have garnered significant attention owing to their unique transition of indirect to direct bandgaps as the number of layers decreases from bulk to a monolayer.[5] In particular, MoS_2 with a monolayer as an electrical channel in a field-effect transistor exhibited both high carrier mobility of 200 $cm^2 V^{-1} s^{-1}$ and an on/off ratio of 10^8 at room temperature.[6] Thus, various applications using MoS_2 nanosheets have been developed such as nonvolatile memory,[7] photodetectors,[8] electrocatalysts,[9] and supercapacitors.[10] The sensitive reactivity of MoS_2 nanosheets to toxic gas molecules has also garnered attention, owing to the high surface area-to-volume ratio of intrinsically thin 2D structures.[11] Sensors for various harmful gases including nitrogen monoxide,[12] carbon monoxide,[13] nitrogen dioxide,[14] ammonia,[15] and volatile organic compounds[16] have been reported using MoS_2 nanosheet-based sensing materials.

Meanwhile, the sensitive detection of hydrogen gas (H_2), a promising candidate for alternative clean energy source, has become necessary for preemptive prevention of potential explosions due to leakage; in this regard, many MoS_2-based H_2 sensors have been reported.[17–22] However, pristine MoS_2 exhibits extremely low sensitivity to nonpolar H_2.[19] One of the approaches for endowing MoS_2 with reactivity to H_2 is the decoration of noble metal catalysts onto the MoS_2 surface. Several metal catalyst-decorated MoS_2 sensors, including palladium,[23–25] gold,[26] platinum (Pt),[27,28] and alloys,[29] have been used for H_2 detection. In particular, Pt is well known to be effective for the sensitive

* Corresponding authorsat: Department of Manufacturing Systems and Design Engineering, Seoul National University of Science and Technology, 232 Gongneung-ro, Nowon-gu, Seoul, 01811, Republic of Korea.
E-mail addresses: kimjb@yonsei.ac.kr (J. Kim), jihwanan@seoultech.ac.kr (J. An).
[1] These authors equally contributed to this work.

https://doi.org/10.1016/j.apsusc.2021.151256
Received 17 June 2021; Received in revised form 1 September 2021; Accepted 9 September 2021
Available online 20 September 2021

detection of H_2 among various noble metal catalysts because of the spillover effect of H_2 on the Pt catalyst, which involves the dissociation of H_2 molecules to reactive atoms and their spread onto a support material.[30] To effectively induce the spillover effect of H_2, the crucial aspects are the areal coverage and the size of Pt nanoparticles on the surface of the sensing material. It was reported that a high sensitivity to a gas was achieved when the areal coverage of metal catalysts on a sensing material was approximately a half of the total surface area.[31] Meanwhile, in terms of the geometry of metal catalysts, small size and uniform distribution of nanoparticles would be beneficial for sensitive detection. This is because a higher number of dissociated hydrogen atoms would be effectively transferred to the sensing material, thereby increasing their reaction probability with oxygen ions.

Accordingly, atomic layer deposition (ALD) could be an interesting and effective technique for introducing highly dense fine nanoparticles on MoS_2 nanosheets to fabricate sensors. ALD, a modified form of chemical vapor deposition (CVD), is based on a unique reaction mechanism, known as self-limited surface saturation, which results in superior process features compared with conventional physical vapor deposition (PVD), or wet methods, namely, atomic-level control of thickness and chemical composition and excellent uniformity.[32,33] More interestingly, during the nucleation period (i.e., normally in a few tens of cycles of the ALD process), we can fabricate highly dense nanoparticles with large surface areas that may be particularly beneficial for chemical/electrochemical sensor applications.[31,34] If the inert basal surfaces of MoS_2 are properly activated by, for instance, seed layering[35,36] and reactive oxidant[37,38] and/or plasma pretreatment[39,40] for nucleation triggering, the best candidate for small and evenly distributed Pt nanoparticle decoration on the surface of MoS_2 could be the ALD process because it exhibits high controllability of the size and distribution of metal nanoparticles. Nevertheless, to the best of our knowledge, atomic layer-deposited metal-decorated MoS_2-based gas sensors have never been reported.

In this study, we demonstrate the novel application of ALD Pt on a MoS_2-based H_2 gas sensor. We systematically explore the effects of process parameters, such as the number of ALD cycles and oxygen plasma pretreatment, on the morphology of Pt nanoparticles on MoS_2 based on atomic force microscopy (AFM), X-ray photoelectron spectroscopy (XPS), and transmission electron microscopy (TEM). The successful decoration of dense Pt nanoparticles on MoS_2 is demonstrated by combining optimal ALD and plasma pretreatment processes. Additionally, we show that the ALD Pt-decorated MoS_2 sensor has superior H_2-sensing property, i.e., the detection limit down to 2.5 ppm, and propose the H_2-sensing mechanism of the ALD Pt-functionalized MoS_2.

2. Experimental section

2.1. Sample preparation

The sensor fabrication process is illustrated in Fig. 1. Multilayer CVD MoS_2 directly grown on an n-type Si/SiO_2 (300 nm) substrate was purchased for sensor fabrication (Six Carbon Technology, China). To functionalize the MoS_2 surface, oxygen plasma pretreatment was performed in a customized remote inductively coupled plasma chamber. Radio-frequency (RF, 13.56 MHz) plasma was used in an oxygen environment under a pressure of 200 mTorr and power of 50 W at room temperature for 30 s (Figure S1).[39] Pt nanoparticles were deposited in a customized thermal-ALD chamber on the surface of the functionalized MoS_2. For the ALD Pt process, trimethyl(methylcyclopentadienyl) platinum (IV) ($MeCpPtMe_3$) and oxygen gas were used as the precursor and oxidant, respectively. The ALD cycle consisted of a Pt source pulse (1 s), Pt source exposure (10 s), N_2 purge (30 s), O_2 pulse (20 s), and N_2 purge (30 s). The chamber temperature and base pressure were maintained at 250 °C and 0.5 Torr, respectively. The resultant growth rate was ~ 0.5 Å/cycle (Figure S2), and the number of ALD Pt cycles was controlled at 0, 10, 20, and 50 cycles. Hereafter, the samples with and without plasma pretreatment were denoted as PO and PX samples, respectively, along with the number of ALD cycles depicted as n (=0, 10, 20, and 50) (such as PO0/10/20/50 and PX0/10/20/50).

2.2. Material characterization

The oxidation state and chemical composition were characterized through XPS with an analysis area of 200 μm × 200 μm and a step size of 0.05 eV (Al Kα source gun, K-Alpha+, ThermoFisher Scientific). Slight Ar-ion etching (0.5 keV, 5 s) was performed before XPS analysis. To study the number of MoS_2 layers as well as the surface oxidation state, Raman spectroscopy was performed with an Ar-ion laser beam at an excitation wavelength of 514 nm with a spot size of 0.7 μm (LabRam Aramis, Horiba Jobin Yvon). The surface topography was characterized through AFM in non-contact mode with a spot size of 1 μm × 1 μm (Tip: NCHR, Nanosensors, equipment: XE-100, Park Systems). The surface Pt particle nucleation density and size were analyzed through transmission electron microscopy (TEM) with an accelerating voltage of 200 kV (JEM-2010, JEOL).

2.3. H_2 sensing performance evaluation

Cr/Au (5/50 nm) electrodes were deposited on the Pt-decorated MoS_2 via e-beam evaporation through a shadow mask. The shadow

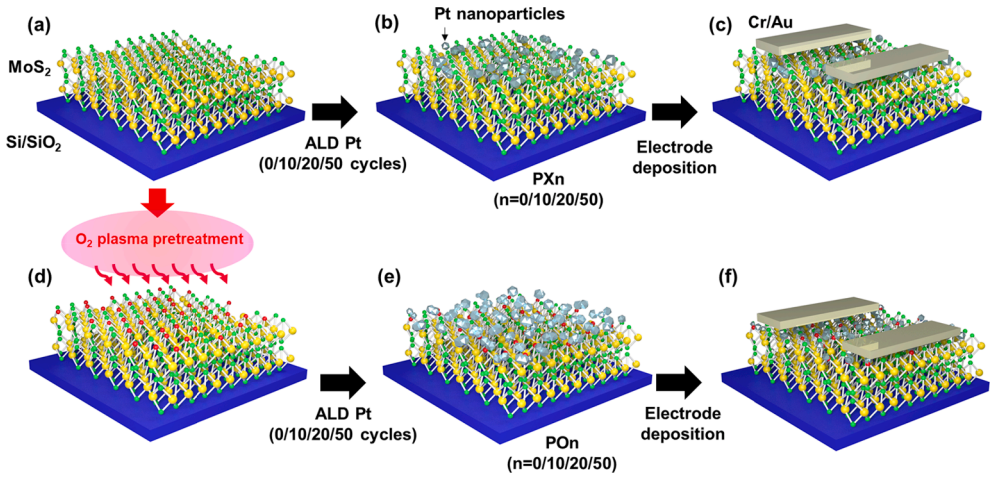

Fig. 1. Schematics of ALD Pt-on-MoS_2 hydrogen sensor fabrication process: (a-b-c) without oxygen plasma pretreatment (PXn (n = 0, 10, 20, 50 cycles)) and (a-d-e-f) with oxygen plasma pretreatment (POn (n = 0, 10, 20, 50 cycles)).

mask was prepared through bulk micromachining using a silicon-on-insulator wafer, resulting in an open hole of interdigitated structures with a 20 μm gap. To evaluate the sensor performance, the fabricated sensors were placed in a quartz-tube chamber connected to mass flow controllers (MFCs), which allowed the generation of H_2 at various concentrations. The other ends of the MFCs were linked with the gas bombs of dry air and H_2. Sensor response was evaluated by monitoring the change in the resistance of the sensor at a constant voltage (1 V) with a computer-controlled source meter (2400, Keithley Instruments). The operating temperature of the sensor was controlled in a furnace where the quartz-tube chamber was on the inner side.

3. Results and discussion

Raman spectra were analyzed to characterize the MoS_2 properties and the change in the oxidation state of the MoS_2 surface before and after oxygen plasma pretreatment. As shown in (Fig. 2**a**), two in-plane E^1_{2g} and out-of-plane A_{1g} vibration peaks were observed at ~ 383 cm^{-1} and ~ 408 cm^{-1}, respectively. The frequency difference was ~ 25 cm^{-1}, indicating the presence of thick (greater than5–6 layers) MoS_2.[41] When analyzed using AFM, the thickness of MoS_2 was approximately 6 nm, which corresponds to ~ 8 layers thick MoS_2 (Figure S3). After oxygen plasma pretreatment, there was no noticeable peak shift or broadening, and only a slight increase in the oxidation-induced peak at approximately 230 cm^{-1} was observed. This implies that oxygen plasma pretreatment on the MoS_2 surface did not significantly etch or damage, but only slightly oxidized the MoS_2 surface forming Mo–O bonds.[42] Surface chemistry of MoS_2 was further investigated through XPS. (Fig. 2b and 2c) show high-resolution XPS spectra near the Mo 3d and S 2p peaks of the PX0 and PO0 surfaces, respectively. Two prominent peaks were observed at 231.6 and 228.4 eV, which correspond to Mo^{4+} 3d doublets in PX0 (i.e., pristine MoS_2) along with the S 2 s peak at 225.7 eV (upper panel in Fig. 2b).[43] However, after oxygen plasma pretreatment, additional oxidation-induced peaks were observed at 235.3 and 232.2 eV, which seem to correspond to Mo^{6+} 3d doublets of the Mo–O bond in MoO_3 crystal (lower panel in Fig. 2b).[44] When the peak areas of Mo^{6+} and Mo^{4+} were quantified, the ratio of Mo^{6+} on the MoS_2 surface was measured to be approximately 57.0 %, which may be the evidence of the transition of the top surface MoS_2 layers into the MoO_3 phase.[39] A similar trend was also observed in the S 2p core-level spectra results. Three peaks were observed at 161.3, 162.5, and 163.7 eV, which correspond to the intrinsic edge S related peak and the S^{2-} 2p doublet peaks, respectively (upper panel in Fig. 2c).[43,45,46] In addition, after the oxygen plasma pretreatment, additional peaks were observed at 169.1 eV and 163.8 eV, which are attributable to sulfate crystals (S–O_3 and S–O_2) (lower panel in Fig. 2c).[47] Moreover, it should be noted that these oxidation-induced peaks disappeared after only 5 s of etching (Ar, 0.5 keV). (Figure S4) Thus, it can be argued that oxygen plasma-induced phase transition is applied to only the top surface layer while minimizing damage to the underlying MoS_2 layer. In other words, oxygen plasma species modifies the chemical state of the surface MoS_2 layer, i.e., accommodates the presence of oxygen on the surface and/or forms oxygen plasma-induced dangling bonds, which may consequently facilitate the nucleation in the subsequent ALD process, as will be discussed later.[48]

AFM topographies were analyzed to study the ALD Pt-deposited (0/10/20/50 cycles) surface morphologies with and without oxygen plasma pretreatment on the MoS_2 surface. (Fig. 3) As can be observed in Fig. 3a, the surface of PXn (untreated) was non-uniform and the Pt nanoparticles exhibited island growth, whereas those on POn exhibited enhanced coverage with more homogenous particle growth. (Fig. 3b) Moreover, root-mean-square (RMS) roughness of PX0 was 0.55 ± 0.10 nm, and gradually increased to 1.60 ± 0.18 nm, 1.89 ± 0.29 nm, and 2.40 ± 0.14 nm at 10, 20, and 50 cycles, respectively. In contrast, that of POn increased from 0.50 ± 0.11 nm to 1.15 ± 0.10 nm during the initial 10 cycles. Thereafter, it saturated to 0.95 ± 0.09 nm and 0.80 ± 0.12 nm

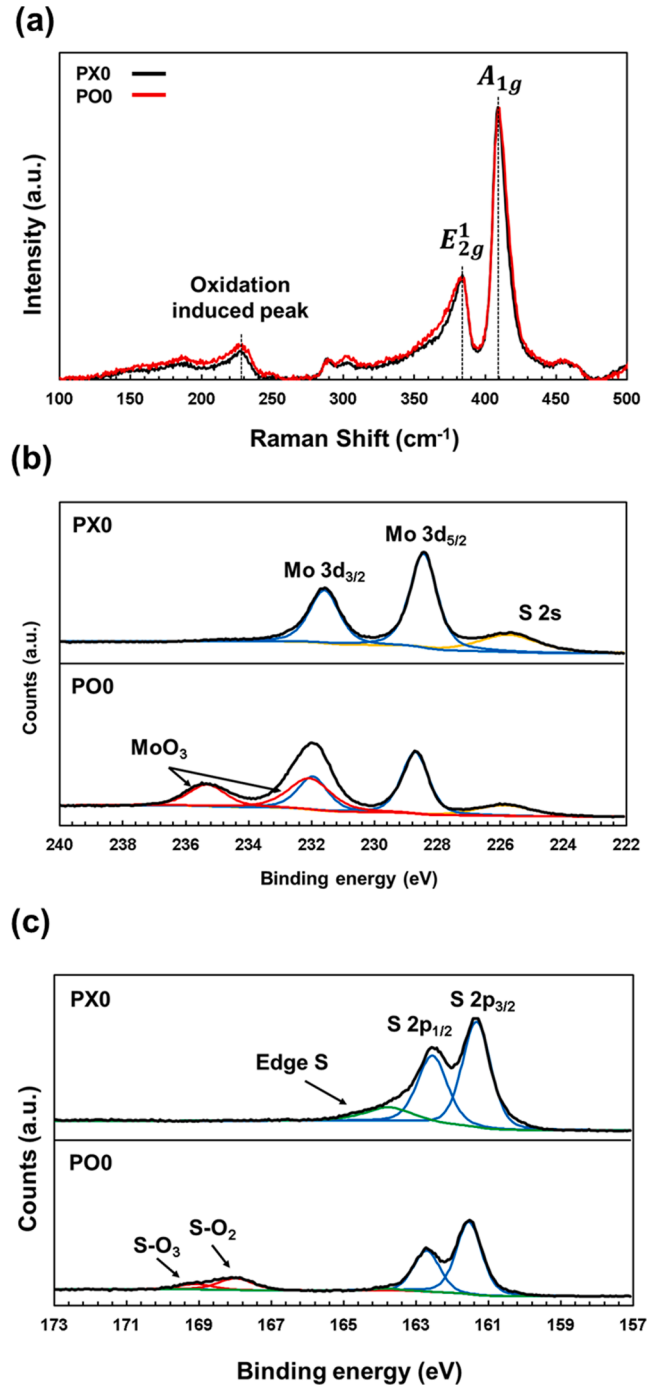

Fig. 2. (a) Raman spectra of MoS_2 surface without/with oxygen plasma treatment (PX0 and PO0) and high-resolution XPS spectra of MoS_2 without/with oxygen plasma treatment (PX0 and PO0) near (b) Mo 3d and (c) S 2p peaks.

at 20 and 50 cycles, respectively, indicating the possibility of more uniform Pt growth with better surface coverage. (Fig. 3c) TEM images on ALD Pt-deposited MoS_2 flakes additionally provide more detailed insight into the effect of oxygen plasma pretreatment on Pt nanoparticles morphology (Figure S5). Similar to previous reports,[49,50] ALD Pt nanoparticles preferentially grew at edge sites and rare nucleation was observed at basal planes in PX10 (untreated) owing to the chemically inert nature of the basal plane (Figure S5a). However, after the oxygen plasma pretreatment followed by ALD, densely distributed Pt particles grew on basal planes (Figure S5b). The average sizes of the Pt

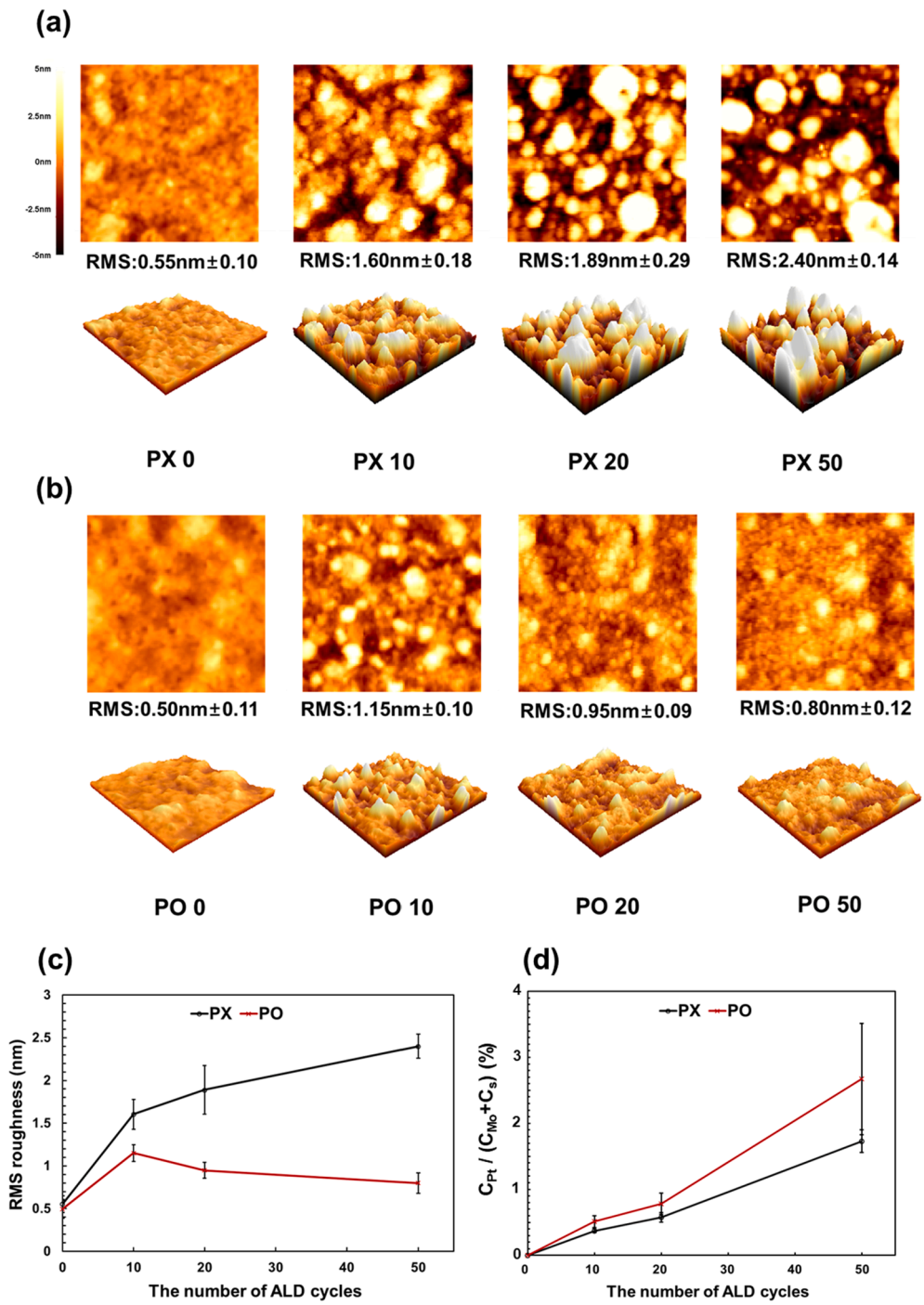

Fig. 3. AFM topography images of MoS_2 surface after 0/10/20/50 ALD Pt cycles (a) without oxygen plasma pretreatment (PXn), (b) with oxygen plasma pretreatment (POn), and (c) the RMS roughness summary. (These images were cropped to 200 nm × 200 nm size from raw 1 μm × 1 μm images.) (d) Relative compositional ratio of Pt and (Mo + S) contents (at%) on MoS_2 surface without/with oxygen plasma treatment based on XPS analysis.

nanoparticles on basal planes were 0.85 ± 0.28 nm in PX10 and 0.93 ± 0.27 nm in PO10; more importantly, the number of particles in PO10 was larger than that in PX10 approximately by a factor of 2 (81 (PX10) vs.153 (PO10) particles in 40 × 40 nm^2), which indicates a more facile and simultaneous nucleation of ALD Pt nanoparticles at an early stage. Moreover, Fig. 3d shows the compositional ratio of Pt-to-Mo/S (i.e., C_{Pt} (at. %)/(C_{Mo} + C_S)(at. %)) in the PXn and POn samples based on XPS analysis. The compositional ratio difference between PXn and POn was not significant at 10 and 20 cycles, whereas it became more evident at 50 cycles (i.e., 2.7 % at PO50 and 1.7 % at PX50 surfaces). The insufficient dangling bonds on PXn MoS_2 are due to strong in-plane bonding in 2D materials; therefore, initial nucleation in the ALD process may be locally limited to only near defects including edge sites,[50,51] resulting in non-uniform and sparse Pt nanoparticle growth observed in TEM and AFM images.[48] In contrast, oxygen plasma pretreatment modified the surface chemistry of MoS_2, forming additional dangling bonds confirmed through Raman and XPS analysis in POn samples, which resulted in the formation of more uniform-in-size and densely distributed ALD Pt nanoparticles with larger surface area and coverage.[48]

Fig. 4 shows the response of the sensors characterized by the number of ALD cycles with or without plasma pretreatment. Here, the response of the sensor to hydrogen is defined as R_{Air}/R_{H2} because the resistance of

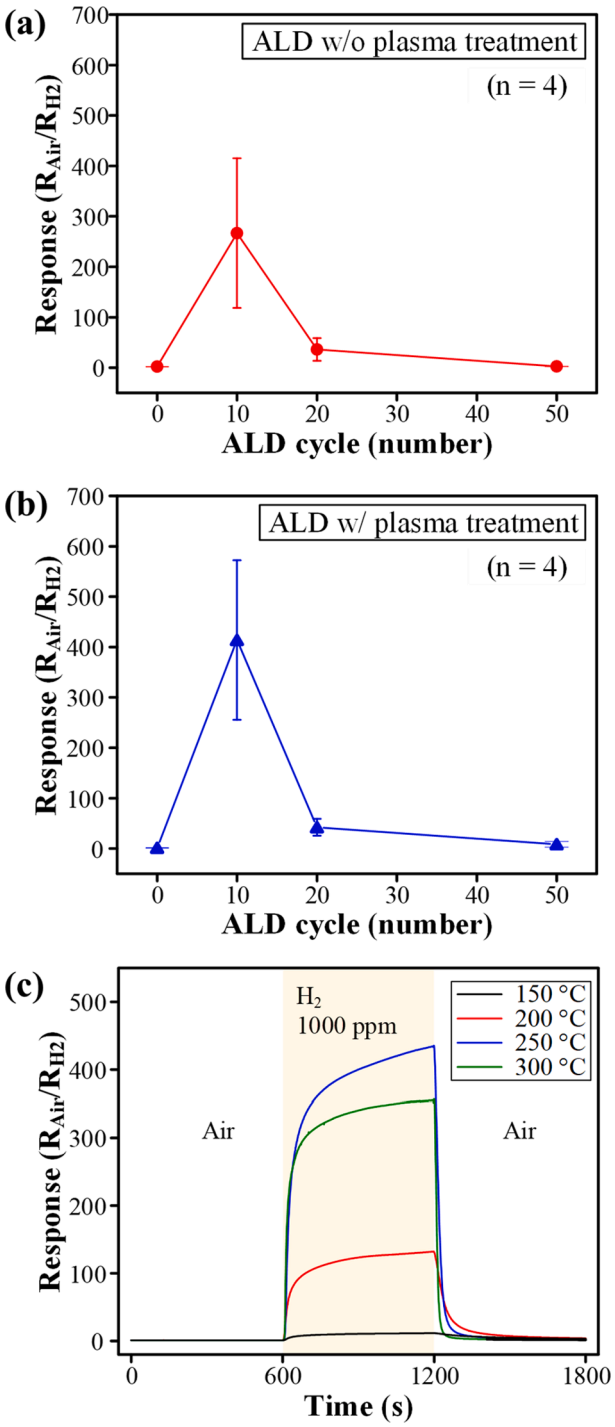

Fig. 4. Response of sensors to 1,000 ppm H_2, characterized with the number of ALD cycles following the (a) absence or (b) presence of the plasma treatment. Pristine MoS_2 shows a very low response to hydrogen regardless of plasma pretreatment. 10 cycled-ALD Pt-decorated MoS_2 with the plasma pretreatment exhibits the highest response. This would indicate that even distribution of small-sized Pt catalysts was formed when 10 cycled ALD was performed. (c) 1,000 ppm H_2 response of 10 cycled-ALD Pt decorated MoS_2 with plasma pretreatment according to operating temperatures.

the sensor decreases when exposed to H_2, where R_{Air} and R_{H2} denote the resistance before and during the exposure to H_2, respectively. The sensor response was evaluated at an operating temperature of 250 °C to demonstrate the difference in sensor response with the varying number of ALD cycles. The response of ALD Pt-decorated MoS_2 to 1,000 ppm H_2 without and with plasma pretreatment is presented in Fig. 4a and 4b, respectively. The average responses of Pt-decorated MoS_2 to 1,000 ppm H_2 were 1.54/2.02 (with/without plasma pretreatment), 414/267, 42.2/36.2, and 8.37/2.69, when the number of ALD cycles was 0, 10, 20, and 50, respectively. With Pt decoration via ALD on MoS_2, however, the sensor exhibited remarkable enhancement in response to H_2, compared with the results of pristine MoS_2 one (please see Figure S6 for transient response of pristine MoS_2 to 1,000 ppm H_2), owing to the catalytic effect of the ALD Pt. The sensors prepared with 10-cycle ALD Pt on MoS_2 showed an average change in the resistance of more than 200 times, regardless of the plasma pretreatment. This result indicates that our approach using the ALD as the decoration method of the noble metal on MoS_2 surface is highly advantageous for achieving high sensitivity to target gas. In addition, it shows that the precisely controlled amount of Pt catalyst on MoS_2 surface is crucial for highly sensitive H_2 detection. Meanwhile, PX10 showed lower responses to H_2 than that of PO10. This is because ALD Pt without the plasma pretreatment was grown on the locally limited MoS_2 surface, which was confirmed using AFM and TEM analyses. Thus, this partial growth on the MoS_2 surface could hinder the efficient participation of Pt catalysts in the H_2 sensing reaction, considering that their small sizes and homogeneous distributions are advantageous for gas sensing. In contrast, plasma pretreatment allows a homogenous distribution of ALD Pt on MoS_2, and Pt catalyst nanoparticles become larger homogeneously as the ALD cycle increases. Hence, PO10 exhibited the highest response. This would indicate that homogeneous distribution of small-sized Pt catalysts was grown with 10 cycles, which was also evident with the highest value of RMS roughness from AFM analysis among POn. As the number of cycles increases, the sensor response decreases owing to the excessive amount (or higher surface coverage) of Pt on MoS_2. This excessive decoration of Pt on MoS_2 could hinder the transport of dissociated hydrogen atoms to the MoS_2 channel owing to the increased thickness of the catalysts, which hampers the catalytic effect. In addition, the open surface of MoS_2 decreases owing to the increased region of covered Pt. This could also be disadvantageous for gas sensing considering that a high sensitivity was achieved when the covered region of metal catalysts on the sensing material was approximately a half of the total surface area of the sensing material.[31] The response of PO10 to different temperatures as the H_2 concentration was fixed at 1,000 ppm is shown in Fig. 4c. The sensor exhibited the highest response when the operating temperature was 250 °C. An optimal temperature of the sensor is observed because the desorption rate of reacted by-products becomes higher than the adsorption rate of target gas as the temperature increases.[52]

The transient responses of the sensor upon exposure to hydrogen at various concentrations are depicted in Fig. 5. This was evaluated using the PO10 sensor, which exhibited the highest response at an operating temperature of 250 °C. Fig. 5a shows the response of the sensor upon repeated exposures to 1,000 ppm H_2 for three cycles, where the sensor responses do not show significant differences. This indicates that the presented approach can achieve high reliability even on repeated exposures to H_2. Fig. 5b displays the transient response upon exposure to hydrogen at several different concentrations ranging from 1,000 to 100 ppm. The relative change in response decreased as the concentration decreased. This confirms that the change in the sensor response was derived from the charge transfer between the hydrogen molecules and Pt-decorated MoS_2. The sensor response to hydrogen at relatively low concentrations is shown in (Fig. 5c). Likewise, the relative change in response decreased as the concentration decreased. The inset of (Fig. 5c) indicates the enlargement of the sensor response to 2.5 ppm H_2.

(Fig. 6**a**) shows the long-term stability of the sensor. The used sensor was stored in an ambient environment without a particular storage technique. The sensor response to 1,000 ppm H_2 was evaluated after 2 and 4 weeks under the same conditions as the initial measurement. We observed no significant change even after 2 and 4 weeks, i.e., no drastic decrease in response. This result implies that the sensor exhibits high reliability over a long period of time with the ambient environment. The

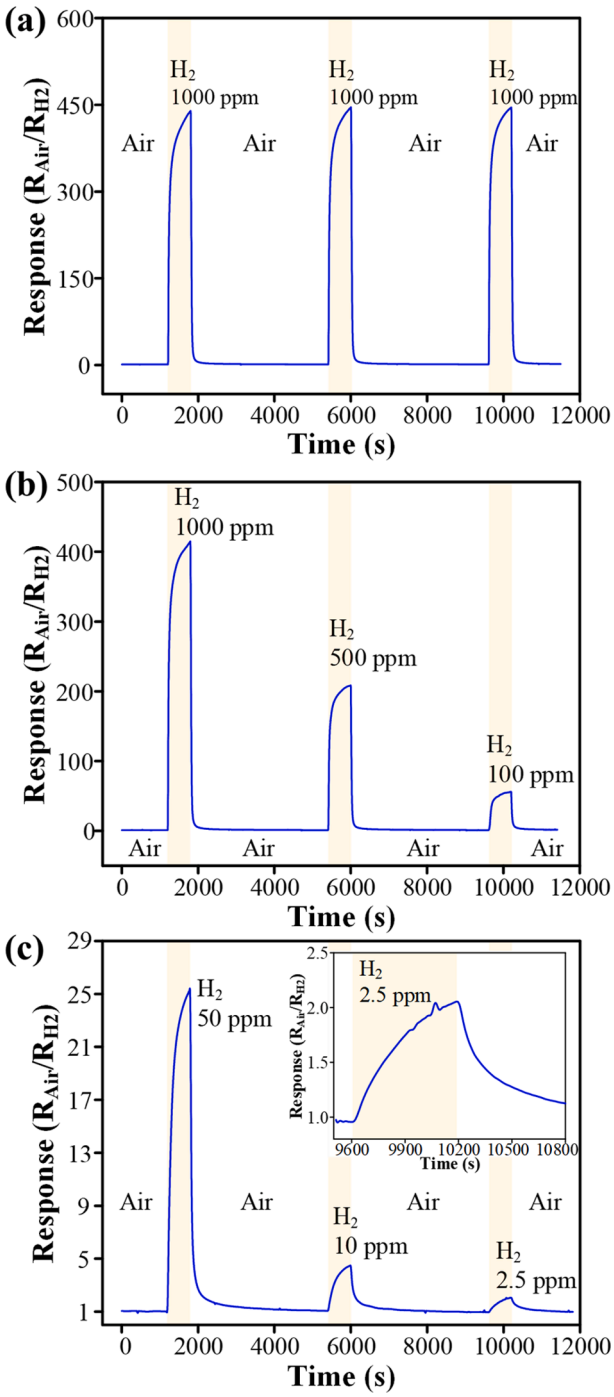

Fig. 5. (a) Transient response of sensor (PO10) upon repeated exposure to 1,000 ppm hydrogen. The sensor response showed no so significant difference on each of several exposures to 1,000 ppm H_2. Transient response of sensor on exposure to hydrogen at various concentrations (b) from 1,000 ppm to 100 ppm and (c) from 50 ppm to 2.5 ppm. Inset of (c) shows the enlargement of the sensor response to 2.5 ppm H_2. The measurement was conducted at an operating temperature of 250 °C.

sensor selectivity to other gas species is presented in (Fig. 6b). The concentrations of the tested gas species were fixed to 1,000 ppm for a fair comparison. Although the sensor sensitively reacts with ammonia to some extent, the response is still lower than that to H_2 at the same concentrations. In addition, the sensor showed low reactivity to other reducing gases such as volatile organic compounds (p-xylene) and alcohol gas (ethanol) when compared with that of H_2. Furthermore, the sensor exhibited extremely low sensitivity to the representative oxidizing gas such as NO_2. Hence, our approach using ALD Pt-decorated MoS_2 as the H_2-sensing material is highly advantageous for achieving high selectivity.

A detailed H_2 sensing mechanism is proposed in Fig. 7. Oxygen molecules dissociate on the surface of the MoS_2 substrate when air is introduced to the sensor, resulting in the formation of oxygen ions (O_2^- and O^-) at elevated temperatures.[53] When H_2 is exposed to the sensor, the decorated Pt facilitates the dissociation of H_2, thereby forming reactive hydrogen atoms and spreading them near the MoS_2 channel.[27] This is known as the spillover effect of Pt catalyst with respect to H_2 sensing.[30] Thereafter, the reactive hydrogen atoms transferred to the MoS_2 channel react with oxygen ions on the surface, thus producing water molecules. This reaction induces the electrons originally captured by oxygen molecules to be transferred to the MoS_2 channel. This results in increase in current in the MoS_2 channel when exposed to H_2.

Table 1 shows a comparison of the sensor performance of metal-decorated MoS_2 channel-based H_2 sensors.[19,23–29] In general, n- and p- type sensing materials show the decrease and increase in resistance, respectively, when exposed to H_2, the reducing gas. Hence, many reported studies use the sensor resistance while exposed to a reducing gas as the denominator and numerator when calculating the response of the n- and p-type sensing material, respectively. Thus, we additionally present the recalculated response in Table 1 to show the ratio of resistance in air/N_2 to H_2 or vice versa. This results in the magnitude of response above 1, making it easier to intuitionally grasp the relative change in resistance. Although a fair comparison for the response (sensitivity) is difficult because of the difference at target concentrations in reported studies, a relative change in resistance of the proposed sensing material was more than 400 times when exposed to 1,000 ppm H_2. In addition, we achieved a notable limit of H_2 detection down to 2.5 ppm, as shown in (Fig. 5c). This indicates that our approach, using ALD as a decoration method for Pt on MoS_2 with plasma pretreatment, is a highly advantageous method used for metal decoration to achieve high sensitivity and a low detection limit. This sensitive detection might be due to the homogeneous distribution of small deposited Pt catalysts on the MoS_2 channel. This is because there are more chances for dissociated hydrogen atoms to be effectively transferred to MoS_2 upon exposure to hydrogen even at low concentrations. In addition, the thickness of Pt after 10 cycles of ALD is estimated to be < 1 nm from Figure S2, which indicates that highly sensitive H_2 detection is efficiently achieved with minimal amounts of catalysts. Furthermore, utilizing a highly controllable ALD process as the Pt decoration method can also be beneficial for the formation of intimate chemical bonding between MoS_2 and the catalyst, unlike PVD which exhibits problems such as evaporation or sputtering. This intimate chemical bonding would induce efficient charge transfer between the deposited Pt and MoS_2 channels.[54] Meanwhile, the fabricated sensing materials should be integrated and operated with a micro-heater for practical applications. This technique is being further studied, including the transfer of CVD MoS_2, fabrication of a micro-heater, ALD process for metal decoration, and the integration of these processes.

4. Conclusion

We studied Pt-decorated MoS_2 via ALD and its novel application to a H_2 sensor. Oxygen plasma pretreatment on MoS_2 allowed functionalization of the initial nucleation sites during the ALD reaction, resulting in a homogeneously distributed decoration with Pt nanoparticles. The growth mechanisms of Pt via ALD with and without plasma pretreatment on MoS_2 were experimentally studied through Raman, XPS, TEM, and AFM analyses. We also characterized the H_2 sensing properties of Pt-decorated MoS_2 with the number of ALD cycles following the detection of the presence or absence of plasma pretreatment. Pt-decorated MoS_2 via ALD (10 cycles) with plasma pretreatment showed the highest response to 1,000 ppm H_2 with a relative change of approximately more

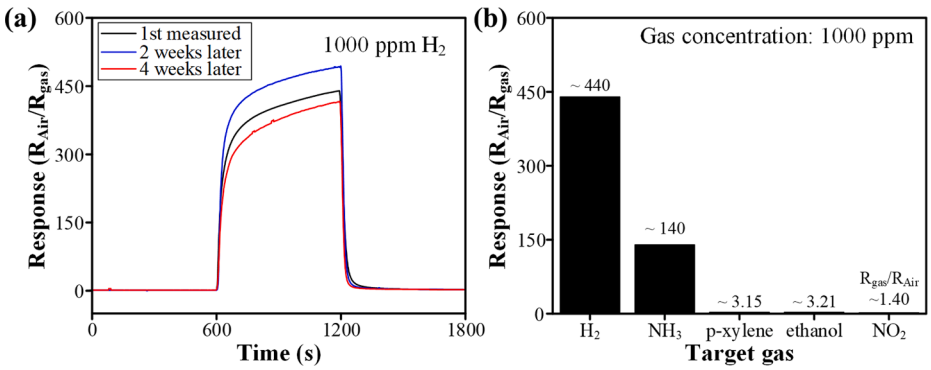

Fig. 6. (a) Long-term stability of the sensor on the exposure to 1,000 ppm H_2. No significant change is observed even after 2 and 4 weeks, such as a drastic decrease in response. This result implies that the sensor exhibits high reliability over a long period of time with the ambient environment. (b) Selectivity of the sensor to other gas species. The sensor showed low reactivity to other reducing gases such as ammonia, volatile organic compounds (p-xylene) and alcohol gas (ethanol) when compared with that to H_2. Furthermore, the sensor exhibited extremely low sensitivity to the representative oxidizing gas such as NO_2. It shows a highly advantageous aspect of our approach using ALD Pt-decorated MoS2 as H_2-sensing material for achieving high selectivity.

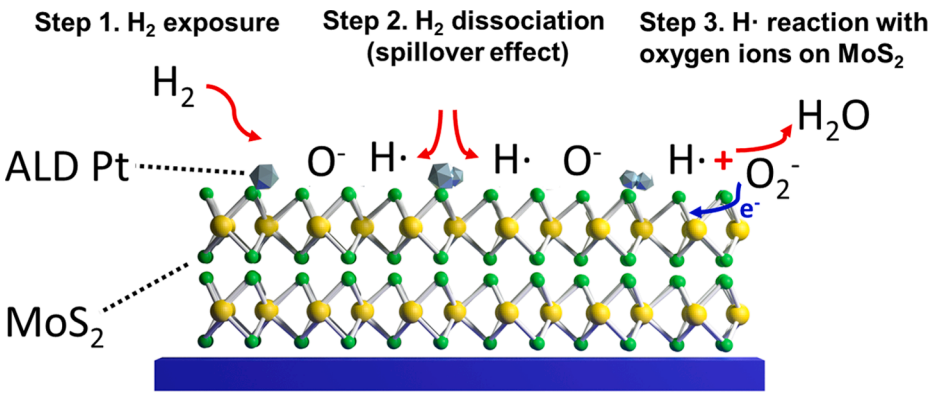

Fig. 7. Detailed H_2 sensing mechanism of ALD-Pt decorated MoS_2 sensor. When hydrogen gas is exposed to the sensor, decorated Pt facilitates the dissociation of H_2, forming reactive hydrogen atom (H•) and spreading them to near MoS_2 channel. This is known as the spillover effect of Pt catalyst regarding H_2 sensing. Then, the transferred reactive hydrogen atoms to MoS_2 channel react with oxygen ions on the surface of it, thereby producing water molecules. This reaction induces that electrons originally captured by oxygen molecules are transferred to MoS_2 channel.

Table 1
Comparison between metal-decorated MoS_2 channel-based H_2 sensors.

Sensing material	Concentration	Response Def.	Response	Limit of detection	Operating Temperature	Reference
Pd-functionalized MoS_2 nanosheet	10000 ppm	(R_{H2}-R_{Air}) /R_{Air} or [R_{H2}/R_{Air}]	0.353 or [1.353]	50 ppm	RT	19
MoS_2 nanosheet–Pd NP composite	50000 ppm	R_{N2}/R_{H2}	10	500 ppm	RT	23
Pd NP functionalized edge-enriched MoS_2 thin film	500 ppm	(R_{H2}-R_{Air}) /R_{Air} or [R_{H2}/R_{Air}]	0.337 Or [1.337]	10 ppm	RT	24
Pd nanocluster-MoS_2 heterostructure	140 ppm	(R_{H2}-R_{Air}) /R_{Air} or [R_{H2}/R_{Air}]	0.17 Or [1.17]	20 ppm	RT (w/ light)	25
Hierarchical flower-like Au-MoS_2 microspheres	30 ppm	R_{Air}/R_{H2}	8.48	30 ppm	175 °C	26
Hollow structure of Pt-decorated MoS_2	40000 ppm	(R_{H2}-R_{Air}) /R_{Air} or [R_{H2}/R_{Air}]	0.12 Or [1.12]	500 ppm	RT	27
MoS_2–Pt nanoparticle composite	100 ppm	R_{Air}/R_{H2}	10	10 ppm	150 °C	28
Multi-component (Ag–Au–Cu–Pd–Pt) alloy NP-decorated MoS_2	1000 ppm	(R_{H2}-R_{Air}) /R_{Air} or [R_{H2}/R_{Air}]	0.32 Or [1.32]	500 ppm	80 °C	29
ALD Pt-decorated MoS_2 nanosheet	**1000 ppm**	**R_{Air}/R_{H2}**	**440**	**2.5 ppm**	**250 °C**	**This work**

than 400 times resistance. The fabricated sensor achieved H_2 detection at several different concentrations ranging from 1,000 to 2.5 ppm. Notably, this detection limit is the lowest among metal-decorated MoS_2-based H_2 sensors, indicating that our approach using ALD and plasma pretreatment as the decoration method of metal catalysts on MoS_2 is highly advantageous. In addition, the H_2 sensing mechanism of the fabricated sensor was proposed owing to the spillover effect of the deposited Pt catalysts on MoS_2. Given the high sensitivity to H_2 and homogenous growth of Pt catalysts on functionalized MoS_2, our approach is expected to be a promising solution for the decoration of metal catalysts on 2D materials to fabricate highly sensitive gas sensors.

CRediT authorship contribution statement

Sungje Lee: Conceptualization, Methodology, Investigation, Visualization, Writing–original draft. **Yunsung Kang:** Conceptualization, Methodology, Investigation, Visualization, Writing–original draft. **Jaehyeong Lee:** Methodology, Investigation. **Jingyung Kim:** Methodology, Investigation. **Jeong Woo Shin:** Methodology, Investigation. **Sangjun Sim:** Methodology, Investigation. **Dohyun Go:** Methodology, Investigation. **Eunhwan Jo:** Methodology, Investigation. **Seunghyeon Kye:** Methodology, Investigation. **Jongbaeg Kim:** Conceptualization, Supervision, Writing – review & editing, Funding acquisition. **Jihwan An:** Conceptualization, Supervision, Writing – review & editing, Funding

acquisition.

Declaration of Competing Interest

The authors declare that they have no known competing financial interests or personal relationships that could have appeared to influence the work reported in this paper.

Acknowledgement

J. An acknowledges the financial support from Nano-Convergence Foundation funded by the Ministry of Trade, Industry and Energy (MOTIE) of Korea (No.20000272) and National Research Foundation of Korea (NRF) funded by the Korea government (MSIP) (No. NRF-2018R1C1B6001150). J. Kim also acknowledges the support from Brain Convergence Research Program of the National Research Foundation (NRF) funded by the Korean government (MSIT) (No. NRF-2019M3E5D2A01063814). We thank Ji Yoon Shin and Prof. Tae Hoon Lee for the help in AFM measurement.

Appendix A. Supplementary material

Supplementary data to this article can be found online at https://doi.org/10.1016/j.apsusc.2021.151256.

References

[1] R. Mas-Balleste, C. Gomez-Navarro, J. Gomez-Herrero, F. Zamora, Nanoscale 3 (2011) 20.
[2] S.J. Kim, K. Choi, B. Lee, Y. Kim, B.H. Hong, Annu Rev Mater Res 45 (2015) 63.
[3] Lin, Z.; McCreary, A.; Briggs, N.; Subramanian, S.; Zhang, K. H.; Sun, Y. F.; Li, X. F.; Borys, N. J.; Yuan, H. T.; Fullerton-Shirey, S. K.; Chernikov, A.; Zhao, H.; McDonnell, S.; Lindenberg, A. M.; Xiao, K.; LeRoy, B. J.; Drndic, M.; Hwang, J. C. M.; Park, J.; Chhowalla, M.; Schaak, R. E.; Javey, A.; Hersam, M. C.; Robinson, J.; Terrones, M., 2d Mater 2016, 3, 042001.
[4] J.C. Lei, X. Zhang, Z. Zhou, Front Phys-Beijing 10 (2015) 276.
[5] A. Splendiani, L. Sun, Y. Zhang, T. Li, J. Kim, C.Y. Chim, G. Galli, F. Wang, Nano Lett 10 (2010) 1271.
[6] B. Radisavljevic, A. Radenovic, J. Brivio, V. Giacometti, A. Kis, Nat Nanotechnol 6 (2011) 147.
[7] H.S. Lee, S.W. Min, M.K. Park, Y.T. Lee, P.J. Jeon, J.H. Kim, S. Ryu, S. Im, Small 8 (2012) 3111.
[8] O. Lopez-Sanchez, D. Lembke, M. Kayci, A. Radenovic, A. Kis, Nat Nanotechnol 8 (2013) 497.
[9] Y. Liu, M. Han, Q. Xiong, S. Zhang, C. Zhao, W. Gong, G. Wang, H. Zhang, H. Zhao, Adv. Energy Mater. 9 (2019) 1803935.
[10] M. Acerce, D. Voiry, M. Chhowalla, Nat Nanotechnol 10 (2015) 313.
[11] T. Pham, G. Li, E. Bekyarova, M.E. Itkis, A. Mulchandani, ACS Nano 13 (2019) 3196.
[12] H. Li, Z. Yin, Q. He, H. Li, X. Huang, G. Lu, D.W. Fam, A.I. Tok, Q. Zhang, H. Zhang, Small 8 (2012) 63.
[13] Q. Zhou, C.X. Hong, Y. Yao, S. Hussain, L.N. Xu, Q.Y. Zhang, Y.G. Gui, M.S. Wang, Mater Res Bull 101 (2018) 132.
[14] D.J. Late, Y.K. Huang, B. Liu, J. Acharya, S.N. Shirodkar, J. Luo, A. Yan, D. Charles, U.V. Waghmare, V.P. Dravid, C.N. Rao, ACS Nano 7 (2013) 4879.
[15] B. Liu, L. Chen, G. Liu, A.N. Abbas, M. Fathi, C. Zhou, ACS Nano 8 (2014) 5304.
[16] J.S. Kim, H.W. Yoo, H.O. Choi, H.T. Jung, Nano Lett 14 (2014) 5941.
[17] V.A. Goltsov, T.N. Veziroglu, Int J Hydrogen Energ 27 (2002) 719.
[18] J.O. Abe, A.P.I. Popoola, E. Ajenifuja, O.M. Popoola, Int. J. Hydrogen Energy 44 (2019) 15072.
[19] D.-H. Baek, J. Kim, Sens. Actuators, B 250 (2017) 686.
[20] A.V. Agrawal, R. Kumar, S. Venkatesan, A. Zakhidov, Z. Zhu, J. Bao, M. Kumar, M. Kumar, Appl. Phys. Lett. 111 (2017), 093102.
[21] A.V. Agrawal, R. Kumar, G. Yang, J. Bao, M. Kumar, M. Kumar, Int. J. Hydrogen Energy 45 (2020) 9268.
[22] Y. Liu, L. Hao, W. Gao, Z. Wu, Y. Lin, G. Li, W. Guo, L. Yu, H. Zeng, J. Zhu, W. Zhang, Sens. Actuators, B 211 (2015) 537.
[23] C. Kuru, C. Choi, A. Kargar, D. Choi, Y.J. Kim, C.H. Liu, S. Yavuz, S. Jin, Adv Sci (Weinh) 2 (2015) 1500004.
[24] J. Jaiswal, P. Tiwari, P. Singh, R. Chandra, Sens. Actuators, B 325 (2020), 128800.
[25] H.D. Mai, S. Jeong, T.K. Nguyen, J.-S. Youn, S. Ahn, C.-M. Park, K.-J. Jeon, ACS Appl. Mater. Interfaces 13 (2021) 14644.
[26] J.X. Wang, Q. Zhou, Z.R. Lu, Z.J. Wei, W. Zeng, Appl Surf Sci 490 (2019) 124.
[27] C.H. Park, W.T. Koo, Y.J. Lee, Y.H. Kim, J. Lee, J.S. Jang, H. Yun, I.D. Kim, B. J. Kim, ACS Nano 14 (2020) 9652.
[28] S.R. Gottam, C.T. Tsai, L.W. Wang, C.T. Wang, C.C. Lin, S.Y. Chu, Appl Surf Sci 506 (2020), 144981.
[29] K.M.B. Urs, N.K. Katiyar, R. Kumar, K. Biswas, A.K. Singh, C.S. Tiwary, V. Kamble, Nanoscale 12 (2020) 11830.
[30] W. Karim, C. Spreafico, A. Kleibert, J. Gobrecht, J. VandeVondele, Y. Ekinci, J. A. van Bokhoven, Nature 541 (2017) 68.
[31] J.-H. Lee, A. Mirzaei, J.-Y. Kim, J.-H. Kim, H.W. Kim, S.S. Kim, Sens. Actuators, B 302 (2020), 127196.
[32] S.M. George, Chem. Rev. 110 (2010) 111.
[33] R.W. Johnson, A. Hultqvist, S.F. Bent, Mater. Today 17 (2014) 236.
[34] Z.U. Abideen, J.-H. Kim, S.S. Kim, Sens. Actuators, B 238 (2017) 374.
[35] G. Lin, M.-Q. Zhao, M. Jia, J. Zhang, P. Cui, L. Wei, H. Zhao, A.T.C. Johnson, L. Gundlach, Y. Zeng, J. Phys. D Appl. Phys. 53 (2019), 105103.
[36] H. Kim, T. Park, S. Park, M. Leem, W. Ahn, H. Lee, C. Lee, E. Lee, S.-J. Jeong, S. Park, Y. Kim, H. Kim, Thin Solid Films 673 (2019) 112.
[37] K.M. Price, K.E. Schauble, F.A. McGuire, D.B. Farmer, A.D. Franklin, ACS Appl Mater Interfaces 9 (2017) 23072.
[38] K.M. Price, S. Najmaei, C.E. Ekuma, R.A. Burke, M. Dubey, A.D. Franklin, ACS Applied Nano Materials 2 (2019) 4085.
[39] J. Yang, S. Kim, W. Choi, S.H. Park, Y. Jung, M.-H. Cho, H. Kim, ACS Appl. Mater. Interfaces 5 (2013) 4739.
[40] Q. Qian, Z. Zhang, M. Hua, G. Tang, J. Lei, F. Lan, Y. Xu, R. Yan, K.J. Chen, Nanotechnology 28 (2017), 175202.
[41] C. Lee, H. Yan, L.E. Brus, T.F. Heinz, J. Hone, S. Ryu, ACS Nano 4 (2010) 2695.
[42] N.R. Kang, H.P. Paudel, M.N. Leuenberger, L. Tetard, S.I. Khondaker, J. Phys. Chem. C 118 (2014) 21258.
[43] L. Zhao, J. Jia, Z. Yang, J. Yu, A. Wang, Y. Sang, W. Zhou, H. Liu, Appl. Catal. B 210 (2017) 290.
[44] Y. Liu, Y.-X. Yu, W.-D. Zhang, The Journal of Physical Chemistry C 117 (2013) 12949.
[45] C. Zhang, Z. Wang, S. Bhoyate, T. Morey, B. Neria, V. Vasiraju, G. Gupta, S. Palchoudhury, P. Kahol, S. Mishra, F. Perez, R. Gupta, C (2017) 3.
[46] C. Backes, R.J. Smith, N. McEvoy, N.C. Berner, D. McCloskey, H.C. Nerl, A. O'Neill, P.J. King, T. Higgins, D. Hanlon, N. Scheuschner, J. Maultzsch, L. Houben, G. S. Duesberg, J.F. Donegan, V. Nicolosi, J.N. Coleman, Nat Commun 5 (2014) 4576.
[47] C.H. Lee, J.M. Yun, S. Lee, S.M. Jo, K. Eom, D.C. Lee, H.I. Joh, T.F. Fuller, Sci Rep 7 (2017) 41190.
[48] H.G. Kim, H.B.R. Leek, Chem. Mater. 29 (2017) 3809.
[49] H. Zhang, D. Chiappe, J. Meersschaut, T. Conard, A. Franquet, T. Nuytten, M. Mannarino, I. Radu, W. Vandervorst, A. Delabie, J. Chem. Phys. 146 (2016), 052810.
[50] S. McDonnell, B. Brennan, A. Azcatl, N. Lu, H. Dong, C. Buie, J. Kim, C.L. Hinkle, M.J. Kim, R.M. Wallace, ACS Nano 7 (2013) 10354.
[51] H. Zhang, D. Chiappe, J. Meersschaut, T. Conard, A. Franquet, T. Nuytten, M. Mannarino, I. Radu, W. Vandervorst, A. Delabie, J Chem Phys 146 (2017), 052810.
[52] M. Bendahan, J. Guérin, R. Boulmani, K. Aguir, Sens. Actuators, B 124 (2007) 24.
[53] Y.J. Zhang, W. Zeng, Y.Q. Li, Appl. Surf. Sci. 455 (2018) 276.
[54] C. Feng, X.H. Mi, D.W. Zhong, W.M. Zhang, Y.P. Liu, D.Y. Fan, M. Li, J.F. Hai, Z. H. Lu, Catalysts 10 (2020).